



# A large conserved family of small-molecule carboxyl methyltransferases identified from microorganisms

Zhi Lin<sup>a,b,1,2</sup>, Zhiwei Hu<sup>a,1</sup>, Linjun Zhou<sup>c</sup>, Benben Liu<sup>a</sup>, Xiaowei Huang<sup>d</sup>, Zixin Deng<sup>a</sup>, and Xudong Qu<sup>a,b,c,2</sup>

Edited by Richard Dixon, University of North Texas, Denton, TX; received January 25, 2023; accepted April 13, 2023

Small-molecule carboxyl methyltransferases (CbMTs) constitute a small proportion of the reported methyltransferases, but they have received extensive attention due to their important physiological functions. Most of the small-molecule CbMTs isolated to date originate from plants and are members of the SABATH family. In this study, we identified a type of CbMT (OPCMT) from a group of *Mycobacteria*, which has a distinct catalytic mechanism from the SABATH methyltransferases. The enzyme contains a large hydrophobic substrate-binding pocket ( $\sim 400 \text{ \AA}^3$ ) and utilizes two conserved residues, Thr20 and Try194, to retain the substrate in a favorable orientation for catalytic transmethylation. The OPCMT-like MTs have a broad substrate scope and can accept diverse carboxylic acids enabling efficient production of methyl esters. They are widely (more than 10,000) distributed in microorganisms, including several well-known pathogens, whereas no related genes are found in humans. In vivo experiments implied that the OPCMT-like MTs was indispensable for *M. neoaurum*, suggesting that these proteins have important physiological functions.

biosynthesis | small molecule carboxyl methyltransferases | steroid | *Mycobacterium*

Methyltransferases (MTs) are ubiquitous in nature and catalyze methyl-transfer reactions to a large variety of substrates, ranging from metabolites to biomacromolecules (1–3). These transformations modulate diverse biological processes, such as signal transduction, transcriptional regulation, and primary and secondary metabolite biosyntheses. Most MTs rely on the cosubstrate *S*-adenosyl-*L*-methionine (SAM) as an electron-deficient methyl donor, transferring a methyl group to a nucleophilic atom through an  $S_N2$  mechanism. According to the methyl-accepting atom of the substrate, MTs are classified as *O*- (1–3), *N*- (4), *C*- (5), *S*- (6), and other acceptor-directed MTs, such as halides (7) and arsenicals (Fig. 1) (8, 9). Among them, *O*-directed MTs (OMTs) can be further divided into hydroxyl OMTs (HOMTs) and carboxyl methyltransferases (CbMTs), which account for  $\sim 54\%$  of total MTs. OMTs often have wide biological significance, thus have been attracted sustained interest (3, 10) e.g., the leucine carboxyl methyltransferases 1 (LCMT1) is related to Alzheimer's disease (11, 12), and catechol OMTs have been a target for developing anti-Parkinson medication (13, 14).

Hitherto, research on CbMTs has been largely focused on protein CbMTs, e.g., leucine carboxyl methyltransferases, while fewer small-molecule CbMTs have been reported (15). Unlike HOMTs that are distributed in all life domains, most small-molecule CbMTs have been identified from plants and belong to the SABATH methyltransferase family (Pfam03492), which plays critical roles in producing active secondary metabolites for plant defense, growth, and reproductive development (16, 17). The substrates of SABATH CbMTs are mostly restricted to fatty acids or small aromatic/cyclic carboxylic acids, such as salicylic acid (SA) (17), benzoic acid (18), (*E*)-cinnamic acid (19), indole-3-acetic acid (IAA) (20), gibberellins (21), jasmonic acid (22), loganic acid (23) and long chain fatty acid (24–27) (Fig. 1 and *SI Appendix*, Fig. S1). SABATH CbMTs generally share considerable sequence similarity and have strict specificity to their natural substrate (15). Due to the efficient esterification of carboxylic substrates under aqueous conditions, significant effort has been devoted in recent decades to the engineering and application of small-molecule CbMTs in the biomethylation of carboxylates for the production of pharmaceuticals (28), biofuels (26), and biomaterials (29), devoting the attention to the development of small-molecule CbMTs in industrial biotechnology.

Recently, we identified two steroidal esters, 3-oxo-4-pregnene-20-carboxyl (3-OPC) methyl ester and 3-oxo-4,17-pregnadiene-20-carboxylic (3-OPDC) methyl ester, from a mutant strain of *Mycolicibacterium neoaurum* CCTCC AB2019054 (*mJTU3*) (30). Their production suggests that one or more small-molecule CbMTs are present in *M. neoaurum*. Here, we performed both in vivo and in vitro studies to identify these enzymes, revealing a large conserved family of small-molecule CbMTs (OPCMT-like MTs) that are distinct from the SABATH family in both sequence identity (<12% identity) and catalytic

## Significance

Small-molecule carboxyl methyltransferases (CbMTs) are critical for modulating biological processes and highly useful in industrial biotechnology; however, they were predominantly restricted to the SABATH family in plants. In this study, the discovery of the 3-OPC carboxyl methyltransferase (OPCMT), which have a distinct catalytic mechanism from SABATH MTs and are widely distributed in microorganisms, significantly broadens the knowledge and availability of small-molecule CbMTs. These methyltransferases (MTs) are indispensable for *M. neoaurum* whereas not found in human beings, suggesting that they could become ideal targets for antibiotics. In addition, their bulky substrate-binding pockets, differentiating them from other MTs, could facilitate the design of specific inhibitors. Finally, the broad substrate specificity and high catalytic efficiency of OPCMTs also provide a valuable tool for the sustainable production of methyl esters.

Author contributions: Z.L., Z.D., and X.Q. designed research; Z.L., Z.H., L.Z., and B.L. performed research; Z.L., Z.H., L.Z., B.L., X.H., and X.Q. analyzed data; and Z. L. and X.Q. wrote the paper.

The authors declare no competing interest.

This article is a PNAS Direct Submission.

Copyright © 2023 the Author(s). Published by PNAS. This article is distributed under [Creative Commons Attribution-NonCommercial-NoDerivatives License 4.0 \(CC BY-NC-ND\)](https://creativecommons.org/licenses/by-nc-nd/4.0/).

<sup>1</sup>Z.L. and Z.H. contributed equally to this work.

<sup>2</sup>To whom correspondence may be addressed. Email: linz@sjtu.edu.cn or quxd19@sjtu.edu.cn.

This article contains supporting information online at <https://www.pnas.org/lookup/suppl/doi:10.1073/pnas.2301389120/-DCSupplemental>.

Published May 8, 2023.

mechanism (Fig. 1). Bioinformatics analysis shows that the gene encoding the OPCMT-like MTs is widely (more than 10,000) and heavily distributed in various microorganisms, including several well-known pathogens, whereas no related gene was found in humans. Moreover, in vivo experiments implied that OPCMT-like MT was indispensable for *M. neoaurum*, suggesting that these proteins have important physiological functions.

## Results

**Identification of MT Genes Responsible for the Methyl Esterification of 3-OPC.** We initially assumed that both the 3-OPC and 3-OPDC methyl esters were synthesized by SABATH methyltransferase. Analysis of the genome of *M. neoaurum* CCTCC AB2019054 revealed 67 MT genes, among which 39 putative MTs were functionally illusive; one sequence, MnMT1, had 27% identity with the SABATH CbMT (1M6E\_1) (17). To verify its function, MnMT1 was overexpressed and purified from *Escherichia coli*. Biochemical assays confirmed that it was inactive to 3-OPC and 3-OPDC, suggesting that the target CbMT did not belong to the SABATH family. Intriguingly, when we used the lysate of *Mycobacterium smegmatis*

mc<sup>2</sup>155, both methyl esters were produced upon the addition of 3-OPC and 3-OPDC, indicating that similar CbMTs were also present in *M. smegmatis*. To further narrow down the identification, we compared the 39 MTs of *M. neoaurum* to the MTs of *M. smegmatis*, identifying 16 homologous protein pairs (MnMT2-17). Among the MnMTs, MnMT2, 3, 4, 5, and 6 showed more than 40% identity with each other (Fig. 2A). The 16 MnMTs were further analyzed via the InterPro database (31), indicating that they could be grouped into six different MT families.

To identify the target CbMT, representative MnMTs (MnMT4, 7, 11, 14, 15, and 17) from each of the six clades were selected for biochemical assays. To our delight, although all others were inactive, MnMT4 showed catalytic activity to convert 3-OPC to 3-OPC methyl ester in the presence of SAM (Fig. 2B and *SI Appendix, Fig. S2*). This transformation failed to proceed in the absence of MnMT4 or SAM, confirming that MnMT4 was a SAM-dependent 3-OPC carboxyl methyltransferase (OPCMT). Considering that MnMT2, 3, 5, and 6 are homologous to MnMT4, we further assayed the methylation activity of 3-OPC. All four proteins converted 3-OPC to 3-OPC methyl ester with moderate to excellent conversion over a 12-h reaction period

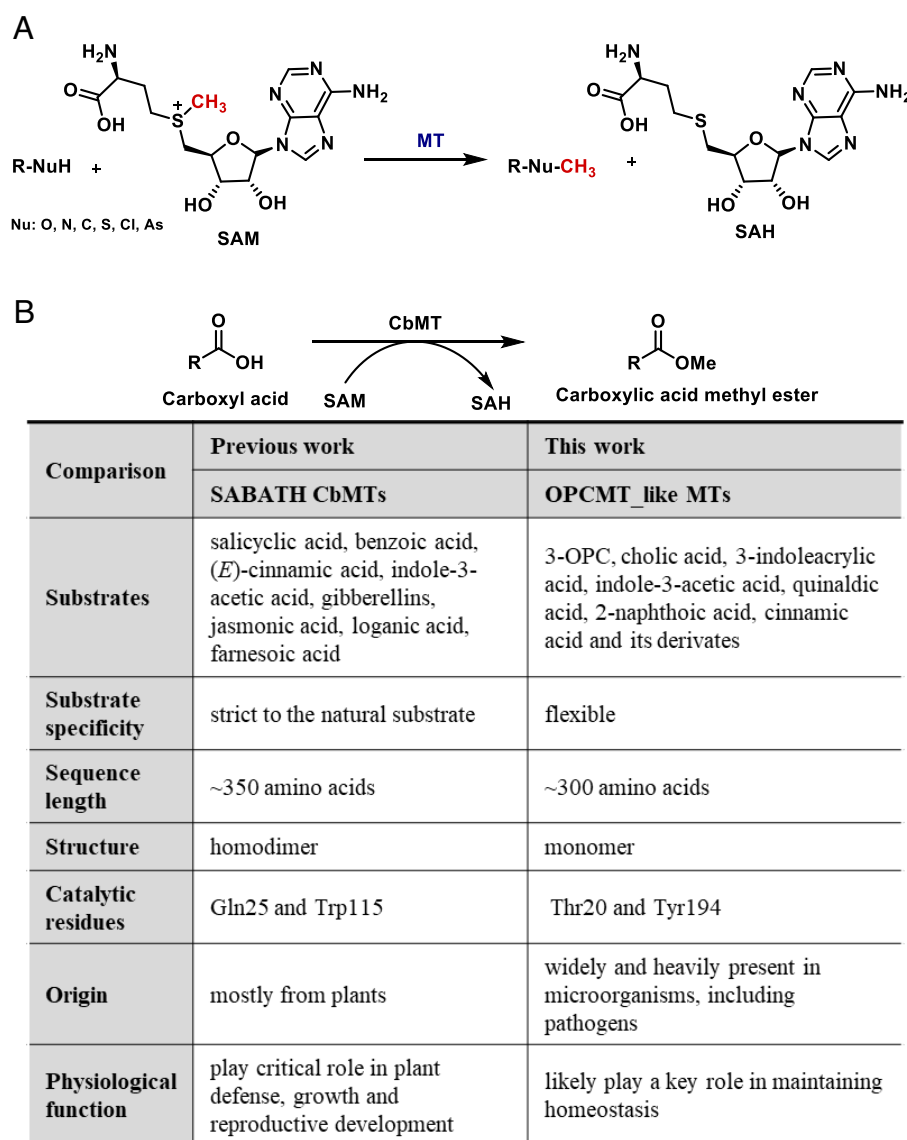


**Fig. 1.** Comparison of small-molecular carboxyl methyltransferases (CbMTs). (A) SAM-dependent MTs. (B) Characterization of SABATH CbMTs and OPCMT-like MTs.

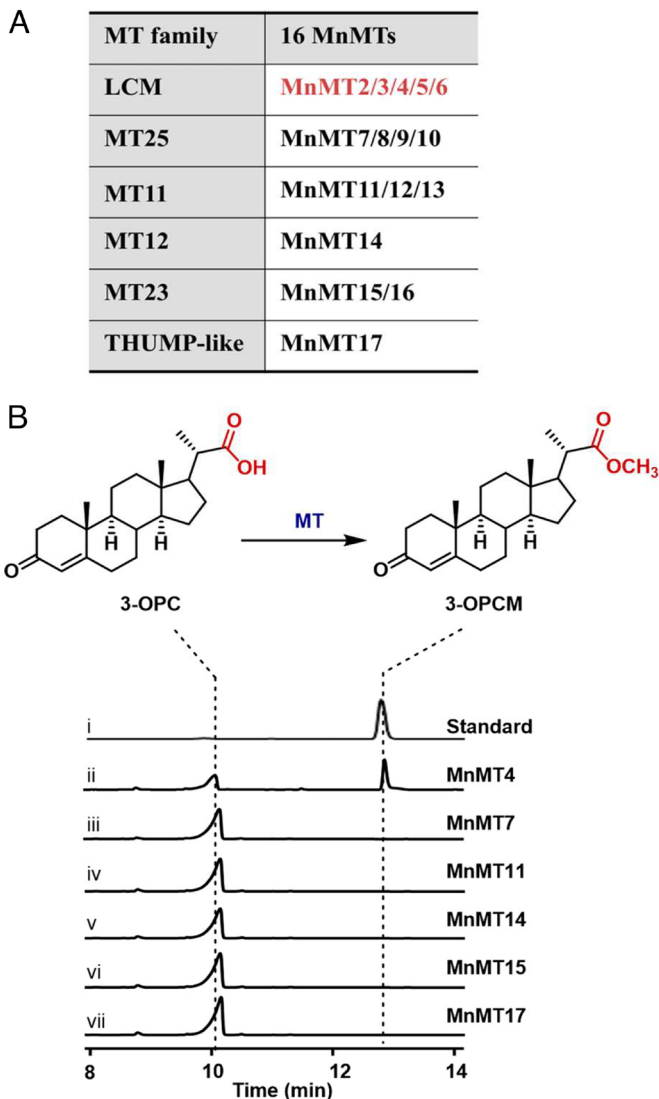


**Fig. 2.** Characterization of MnMT4 as the MT responsible for 3-OPC methylation. (A) Grouping the 16 MTs of *M. neoaurum* CCTCC AB2019054, all of which have homologous proteins in *M. smegmatis* mc<sup>2</sup>155, in the InterPro database, OPCMT\_like MTs are shown in red. (B) Biotransformation of 3-OPC to 3-OPCM using crude recombinant cell lysate. The ID of the six different MT families in InterPro: MT25 (IPR041698); MT11 (IPR013216); MT12 (IPR013217); MT23 (PF13489); LCM (IPR007213); THUMP-like (IPR041497).

(i.e., 98%, 96%, 70%, 75%, and 49% for MnMT4, 2, 6, 5, and 3, respectively).

InterPro analysis indicated that these five proteins belonged to the leucine carboxyl methyltransferase (LCM) fold (IPR007213). LCM was originally discovered as the protein's C-terminal leucine carboxyl methyltransferase (11). The core domains (Rossmann fold) of the LCMs are well conserved to the class I methyltransferases; however, their catalytic mechanisms and substrates are very diverse (11, 12, 32, 33). Considering that MnMT2-6 have no sequence identity to the reported MTs of the LCM family (<20% identity), such as LCMT1 for methylation of the C-terminal leucine residue of serine/threonine phosphatase PP2A in mammals (11, 12) and TcmP for methylation of the C-9 carboxyl group of tetracenomycin E (33), or to the SABATH type CbMTs (<12% identity), we speculated that they may represent a novel type of CbMT, and thus named them OPCMT\_like MTs (*SI Appendix, Fig. S4*).

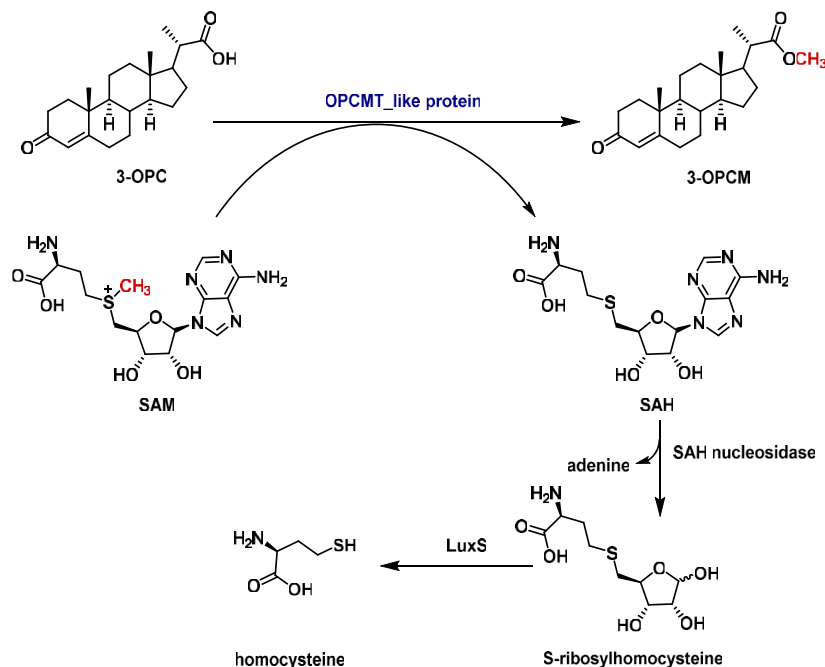
SAH produced in the methyl transfer reaction is known to be a potent feedback inhibitor for most SAM-dependent MTs. To

verify whether OPCMT\_like MTs were inhibited by SAH, we used Fortebio to determine the binding affinity of MnMT4 with SAM and SAH, respectively. The equilibrium dissociation constant ( $K_D$ ) with SAH was nearly three orders of magnitude lower than that with SAM ( $K_D = 2.91 \times 10^{-8}$  M with SAH,  $K_D = 1.84 \times 10^{-5}$  M with SAM), indicating that SAH is a potent inhibitor of MnMT4 (*SI Appendix, Fig. S5*). To alleviate this inhibition, we overexpressed and purified the SAH nucleosidase (EC 3.2.2.9) and *S*-ribosylhomocysteinase LuxS (EC 3.2.1.148) of *E. coli*, which can sequentially hydrolyze SAH to adenine and cleave *S*-ribosylhomocysteine to homocysteine (34, 35). As expected, the addition of SAH nucleosidase and LuxS to the methyl transfer reactions promoted conversion to more than 96% (Figs. 3 and 4 and *SI Appendix, Fig. S7*). Kinetic analysis revealed that the catalytic efficiency of MnMT4 ( $k_{cat}$  at  $765.3 \pm 97.40$  min<sup>-1</sup>,  $K_m$  at  $489 \pm 103.6$   $\mu$ M and  $k_{cat}/K_m = 1.563$   $\mu$ M<sup>-1</sup>min<sup>-1</sup>) was much higher than those of the other four MTs (Fig. 3 and *SI Appendix, Fig. S8*), suggesting that it plays a major role in the synthesis of 3-OPC methyl ester in *M. neoaurum*. In addition, this catalytic efficiency is also far more efficient than the typical values of SABATH MTs, whose  $k_{cat}$  values on SA and IAA are  $5.52 \pm 0.46$  min<sup>-1</sup> and  $1.68 \pm 0.19$  min<sup>-1</sup>, respectively (17).

*M. smegmatis* mc<sup>2</sup>155 has 10 MTs with more than 30% identity with MnMT4. Among them, MsMT1 showed the highest homology (67% identity) to MnMT4. Consistent with the result using *M. smegmatis* cell lysate, MsMT1 showed a very efficient catalytic efficiency on 3-OPC, resulting in up to 100% conversion of OPC after 12 h (*SI Appendix, Fig. S4*). These results demonstrate that the genes encoding OPCMT\_like MTs are heavily distributed in both *M. neoaurum* CCTCC AB2019054 and *M. smegmatis* mc<sup>2</sup>155, which may have a profound effect on the steroid catabolism of these organisms.

**Structure and Catalytic Mechanism of OPCMT\_Like MTs.** We next sought for homologous proteins of MnMT4 in the PDB bank to determine if any protein structures of OPCMT\_like MTs had been reported. This led to the identification of two homologous proteins, ML2640c (PDB ID: 2UYQ) and Rv0731c (PDB ID: 6ID6), which originated from the pathogens *Mycobacterium leprae* and *Mycobacterium tuberculosis* and showed 40% and 39% identity with MnMT4, respectively. Interestingly, the functions of these two proteins remained unrevealed (36); and their structures had been determined, since they were conserved hypothetical proteins in pathogenic *Mycobacteria*. To characterize their catalytic functions, these proteins were overexpressed and purified from *E. coli*. Biochemical assays established that both could completely convert 3-OPC to 3-OPC methyl ester, thus clearly verifying that they were indeed OPCMT\_like CbMTs. Notably, both the OPCMT\_like MTs are monomers, distinct from the conventional CbMTs of the SABATH family that exist as homodimers (17).

The adenosyl moiety of SAM in ML2640c is clearly defined while its amino acid moiety is disordered and invisible (Fig. 5A). Structural superposition of ML2640c and Rv0731c revealed perfect overlap and both showed an *N*-terminal helical domain ( $\alpha_1$  to  $\alpha_4$ ) followed by an  $\alpha/\beta$  C-terminal domain made up of a central  $\beta$ -sheet flanked by  $\alpha$ -helices (Fig. 5B). Their *N*-terminal helical domains are unique and have not been previously observed in other MTs. These domains were presumed to be related to the substrate-binding specificity, while the SAM-binding  $\alpha/\beta$  C-terminal domain is well conserved in SAM-dependent MTs. Structural superposition of the ML2640c-SAM complex and the yeast phosphatase methyltransferase PPM1-SAM complex (PDB: 1RJD) (34) provided a binding model of SAM in the  $\alpha/\beta$  C-terminal domain of ML2640c (Fig. 5C and *SI Appendix, Fig. S9*). According to the model, the



MTs	$k_{cat}$ ( $\text{min}^{-1}$ )	$K_m$ ( $\mu\text{M}$ )	$k_{cat}/K_m$ ( $\mu\text{M}^{-1} \text{min}^{-1}$ )
MnMT2	27.64 ± 1.35	292 ± 42.84	0.095 ± 0.009
MnMT3	8.004 ± 0.99	2825 ± 585.2	0.003 ± 0.0002
<b>MnMT4</b>	<b>765.3 ± 97.40</b>	<b>489.7 ± 103.6</b>	<b>1.56 ± 0.13</b>
MnMT5	12.83 ± 0.91	701.5 ± 132.5	0.018 ± 0.002
MnMT6	3.29 ± 0.19	312.4 ± 54.76	0.011 ± 0.001

**Fig. 3.** Enzymatic kinetic parameters of the OPCMT\_like proteins in *M. neoaurum* CCTCC AB2019054. The most efficient OPCMT\_like protein is shown in red.

adenine of SAM in ML2640c was stabilized by hydrogen-bonding interactions with the Asp164 side chain and the Leu165 main-chain NH, and the ribose moiety of SAM was accommodated by the residues Ala113 and Gly115 between  $\beta_1$  and  $\alpha_5$ , corresponding to

the conserved GxGxG motif between  $\beta_1$  and  $\alpha_A$  in other class I MTs (3). Moreover, the two ribose-OH groups were hydrogen bonded to the carboxylate oxygens of Asp135 and the side-chain residues Arg28, Arg90, while Glu189 could have electrostatic

Substrate	MT	Conversion	Substrate	MT	Conversion	Substrate	MT	Conversion	Substrate	MT	Conversion
	MT4	100%		MT4	84%		MT4	100%		MT4	86%
	MT2	99%		MT2	89%		MT2	100%		MT2	63%
	MT6	98%		MT6	66%		MT6	71%		MT6	89%
	MT5	96%		MT5	82%		MT5	30%		MT5	26%
	MT3	97%		MT3	69%		MT3	< 3%		MT3	< 3%
	MT4	100%		MT4	79%		MT4	74%		MT4	68%
	MT2	95%		MT2	36%		MT2	84%		MT2	94%
	MT6	59%		MT6	37%		MT6	23%		MT6	18%
	MT5	< 1%		MT5	< 1%		MT5	8%		MT5	< 1%
	MT4	93%		MT4	95%		MT4	98%		MT4	89%
	MT2	98%		MT2	88%		MT2	92%		MT2	52%
	MT6	32%		MT6	29%		MT6	69%		MT6	58%
	MT5	16%		MT5	29%		MT5	12%		MT5	13%
	MT4	63%		MT4	< 1%	<b>No conversion</b>					
	MT2	69%		Phenyl maleic acid	Phenyl maleic acid	Hex-2-enoic acid	3-Phenylpropionic acid	Salicylic acid	Benzoic acid	Phenylmalonic acid	Lauric acid
	MT6	26%		Hex-2-enoic acid	Hex-2-enoic acid	3-Phenylpropionic acid	Salicylic acid	Benzoic acid	Phenylmalonic acid	Lauric acid	
	MT5	< 1%		3-Phenylpropionic acid	3-Phenylpropionic acid	Salicylic acid	Salicylic acid	Benzoic acid	Phenylmalonic acid	Lauric acid	
MT3	< 1%	Salicylic acid	Salicylic acid	Benzoic acid	Benzoic acid	Phenylmalonic acid	Phenylmalonic acid	Lauric acid	Lauric acid		

**Fig. 4.** Analysis of the substrate preference of the five OPCMT\_like proteins originating from *M. neoaurum* CCTCC AB2019054. Conversion over 70% are shown in red.

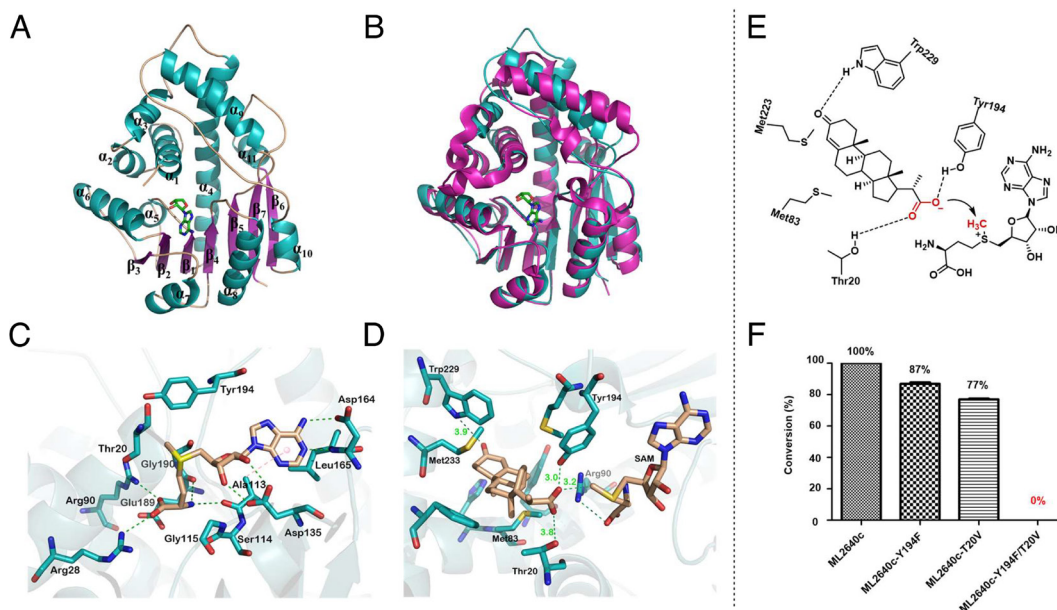


**Fig. 5.** (A) Structure of ML2640c (2U9Q). (B) Structural superposition of ML2640c (blue) and Rv0731c (aubergine). (C) View of the SAM-binding site (the residues are shown in blue sticks, and 3-OPC and SAM are shown in orange sticks). (D) View of the 3-OPC-binding site (the residues are shown in blue sticks, 3-OPC and SAM are shown in orange sticks). (E) Enzymatic mechanism of ML2640c. (F) Comparison of methylation activity of ML2640c and its mutants.

interactions and hydrogen-bonding interactions with the charged tail of SAM (Fig. 5C and *SI Appendix, Fig. S9*). Such SAM-binding modes of ML2640c followed a very similar pattern observed in other known class I MTs structures (3, 37), and the residues in contact with SAM were highly conserved in OPCMT\_like MTs (*SI Appendix, Fig. S10*).

To further clarify the catalytic mechanism of OPCMT\_like MTs, 3-OPC was docked into the SAM-bound ML2640c, and the complex structure was optimized by molecular dynamics (*SI Appendix, Fig. S11*), resulting in a reasonable geometry between the carboxylate oxygen of 3-OPC and the reactive methyl group of SAM. Their distance of 3.2 Å is in the reachable range for methyl transfer. Moreover, 3-OPC is positioned in a large hydrophobic cavity (~400 Å<sup>3</sup>, *SI Appendix, Fig. S11*) composed of the *N*-terminal helical domain ( $\alpha_1$  to  $\alpha_4$ ) and the C-terminal ends of strands  $\beta_4$ ,  $\beta_5$ , and  $\beta_7$  and surrounded by residues Thr20, Tyr194, and Trp229 (Fig. 5D). The hydrophobic side chains of Met83 and Met233 encompass the steroidal framework of 3-OPC and the reactive carboxylate moiety of 3-OPC is secured by hydrogen-bonding interactions with the hydroxyls of Thr20 and Tyr194 (Fig. 5E). Notably, both the Thr20 and Tyr194 are highly conserved in the above OPCMT\_like MTs (*SI Appendix, Fig. S10*). To verify their functional roles, the Thr20 and Tyr194 of ML2640c were mutated to Val and Phe, respectively, and the resulting mutants showed decreased activity toward 3-OPC (Fig. 5F and *SI Appendix, Fig. S12*). When the Thr20 and Tyr194 were simultaneously mutated, ML2640c-T20V/Y194F completely lost its methylation activity toward 3-OPC, demonstrating the essential roles of the residues in catalytic activity. Furthermore, W229 forms a hydrogen bond with the 3-keto group of 3-OPC in ML2640c. This residue is not conserved in the other OPCMT\_like MTs (*SI Appendix, Fig. S10*); mutating it to alanine did not affect its activity (*SI Appendix, Fig. S12*), suggesting that the binding affinity contributed by other residues is sufficient for ML2640c.

To elucidate the functional role of Thr20 and Tyr194 in catalysis, we employed 4-HBC (Fig. 4), an alcohol mimic of 3-OPC, to determine the activity of ML2640c. As 4-HBC has an identical steroidal framework, it was assumed to accommodate the same binding conformation as 3-OPC. Biochemical assays revealed that ML2640c

was completely inactive to 4-HBC, indicating that both Thr20 and Tyr194 might only participate in fixing the carboxyl group of 3-OPC and help in its desolvation, but not act as acid/base catalysts. The carboxyl group of 3-OPC is expected to be ionized to the carboxylate anion in neutral conditions, enabling it to nucleophilically attack the reactive methyl group of SAM for the methyl transfer reaction. This type of proximity and desolvation enzymatic mechanism is also used by the typical CbMTs of the SABATH family (1). However, the CbMTs of the SABATH family use conserved Gln25 and Trp115 as the critical guiding groups for binding the substrate's carboxyl group, and the substrate-binding pocket is much smaller than that of the OPCMT\_like protein (4).

**Substrate Specificity of OPCMT\_Like MTs.** The substrates of the SABATH family are diverse (*SI Appendix, Fig. S1*). In addition to methylating the carboxyl group, they can also methylate the *N* atoms of a few alkaloids, but each MT in the SABATH family has its own unique substrate preference (4). As OPCMT\_like MTs have a very large binding pocket, we questioned whether they would accept other substrates. Therefore, we tested the activities of MnMT2, 3, 4, 5, and 6 on various carboxylates with different scaffolds. Interestingly, MnMT4, 2, and 6 were very promiscuous and accepted cholic acid, 2-naphthioic acid, quinaldic acid, 3-indoleacrylic acid, indole-3-acetic acid, and (*E*)-cinnamic acid derivatives bearing different substitutions (Fig. 4 and *SI Appendix, Tables S4*), while the substrate recognition of MnMT3 and 5 was relatively specific. All five CbMTs preferred to recognize 3-OPC, followed by cholic acid and alkenoic acid (acids with rigid backbones), and they did not recognize the carboxylates with flexible backbones such as hex-2-enoic acid, 3-phenylpropionic acid, and lauric acid or other acids with bulky substituents in the C $\alpha$  or C $\beta$  of the carboxyl group. These results were consistent with their catalytic mode in which the carboxyl group necessitates a suitable conformation to facilitate methyl transfer, while carboxylates with flexible backbones are difficult to fix. Time course experiments demonstrated that the order of substrate range and catalytic efficiency of these five CbMTs was MnMT4 > MnMT2 > MnMT6 > MnMT5 > MnMT3 (*SI Appendix, Table S4*).

Considering the high catalytic efficiency and broad substrate scope, we speculated that CbMTs play an important role in maintaining acid homeostasis in microorganisms, as it is well known that carboxylic acids can inhibit microbial activity by damaging the cell membrane or by decreasing the microbial internal pH (38). In addition, sterols are toxic to mycobacteria such as *M. tuberculosis*, although their catabolism can provide carbon and energy sources for mycobacteria and play a critical role in the survival and pathogenicity of mycobacteria (39, 40). Thus, methylation of sterol acids may be important for maintaining metabolic homeostasis and suppressing toxicological consequences of accumulating sterols. To verify our hypothesis, we initially tested the sensitivity of *M. neoaurum* CCTCC AB2019054 to 3-OPC and cinnamic acid. The minimum inhibitory concentrations (MICs) of 3-OPC and cinnamic acid were 3 mM and 0.6 mM, respectively, indicating that the steroidal acid and cinnamic acid were indeed toxic to *M. neoaurum*.

To elucidate whether OPCMT-like MTs were important in maintaining sterols and acid homeostasis, we attempted to simultaneously inactivate the five encoding genes of OPCMTs in CCTCC AB2019054 using a CRISPR-Cas9-based editing tool (41) but we failed to obtain the target mutant. Therefore, we deleted these genes individually. First, the genes encoding the most active proteins, MnMT4, 2, and 6, were successively knocked out, resulting in the mutant  $\Delta 3mnmmt$  (SI Appendix, Fig. S13). However, the MICs of 3-OPC and cinnamic acid against  $\Delta 3mnmmt$  were similar to those of the wild type, indicating that the remaining two CbMTs, MnMT3 and 5, could compensate for their function. Therefore, the gene encoding MnMT3 was next knocked out based on  $\Delta 3mnmmt$ , resulting in the mutant  $\Delta 4mnmmt$ . As expected, the MICs of 3-OPC and cinnamic acid against  $\Delta 4mnmmt$  were 2 mM and 0.4 mM, respectively, slightly lower than that of the wild type. Interestingly, inactivating the last gene encoding MnMT5 from  $\Delta 4mnmmt$  was not successful, but it was easily knocked out in the wild-type strain (SI Appendix, Fig. S14). Although  $\Delta 4mnmmt$  showed decreased activity in synthesizing 3-OPC methyl ester compared to the wild-type strain, it retained the catalytic activity of Cb-methylation (SI Appendix, Fig. S15), suggesting that the last protein, MnMT5, was still able to confer sufficient Cb-methylation activity. We speculated that the OPCMT-like MTs may be essential in maintaining carboxylic acid homeostasis, and thus at least one OPCMT-like MT is required for bacterial survival.

**The Gene Encoding OPCMT-Like MT Is Widely Present in Various Microorganisms.** To explore the distribution of OPCMT-like MTs, ML2640c was used as a probe to retrieve its homologues via UniProt. To our surprise, the results showed that there were at least 10,000 ML2640c homologues (>30% identity) in various organisms, and most sequences were about 300 amino acids in length (about 50 amino acids shorter than the sequences of CbMTs in the SABATH family), suggesting that OPCMT-like MTs may be a large conserved family. Further analysis indicated that the homologous proteins of ML2640c are widely present in *Mycobacterium* spp. (NCBI taxid: 1,763, >5,000) and some related species, such as *Streptomyces* spp. (NCBI taxid: 1,883, >2,000), *Nocardia* spp. (NCBI taxid: 1,817, >400), *Rhodococcus* spp. (NCBI taxid: 1,827, >200), *Amycolatopsis* spp. (NCBI taxid: 1,813, >150), *Chlamydomonas* spp. (NCBI taxid: 3,052, >50), and *Kitasatospora* spp. (NCBI taxid: 2,063, >50). Small numbers of these homologs exist in other species, including plants and fungi, but are lacking in the kingdom of Animalia, such as in humans.

Randomly aligning more than 5,000 homologous sequences (>30% identity) originating from different species showed that

the Thr20 residue responsible for binding the carboxyl group was conserved among these homologs as well as the residues responsible for binding the methyl donor SAM (Arg28, Arg90, Ala113, Gly115, Ser114, Asp135, Asp164, Leu165, Glu189, and Gly190) (Fig. 6 and SI Appendix, Figs. S11 and S16). Only a few of these homologous proteins had Phe replacing the residue Tyr at 194, but according to the above mutation experiments, the methylation activity of mutant ML2640c-Y195F remained active (Fig. 5F), indicating that these OPCMT-like MTs were still catalytically active. Therefore, both residues Thr20 and Tyr/Phe194 can be recognized as landmarks of the OPCMT-like MTs, as these are distinct from the signature residues (Gln25 and Trp115) of the SABATH family (17).

The OPCMT-like MT encoding genes are widely present and abundant in many well-known pathogens. For instance, there are more than 1,500 OPCMT-like MT encoding genes in the *Mycobacterium tuberculosis* complex (NCBI taxid: 77,643) and the *Mycobacterium avium* complex (MAC) (NCBI taxid: 120,793), 20 in *M. avium* 104 (NCBI taxid: 243,243), and 27 in *Mycobacterium ulcerans* (NCBI taxid: 1,809). Although the physiological function of OPCMT-like proteins in these pathogens remains uncertain, the in vivo experiments implied that OPCMT-like MTs were indispensable for *M. neoaurum*, suggesting that they might be crucial in maintaining microbial physiological activity. The conserved OPCMT-like proteins are not found in the kingdom Animalia, implying that they could be developed as spectral antimicrobial drug targets for both humans and animals.

## Discussion

Carboxyl methyl esterification is an important and ubiquitous reaction in both living organisms and in industrial applications. (15) Due to the dramatic changes in physicochemical properties, methyl esterification of small-molecular acids catalyzed by CbMTs is often pivotal to maintaining metabolic homeostasis and modulating biological processes in nature. Previous studies have shown that the SABATH methyltransferase family is the best characterized and well-defined CbMT family; the enzymes have been largely identified from plants and are responsible for the formation of various volatile methyl esters that play significant roles in the defense, growth, and reproductive development of plants (16, 17). A few members of the SABATH methyltransferase family have shown significant potential in the industrial production of pharmaceuticals, biofuels, and biomaterials (26, 28, 29). Although the substrates catalyzed by the SABATH CbMTs are diverse and the protein sequences are considerably similar, members of this family generally have strict specificity to their natural substrate. Unlike the SABATH CbMTs, the CbMTs identified herein are widely present in microorganisms rather than in plants, and all have a large binding pocket to accept 3-OPC as their substrate. Moreover, this family is also very flexible regarding other substrates, such as cholic acid, 2-naphthioic acid, quinaldic acid, 3-indoleacrylic acid, indole-3-acetic acid, and (*E*)-cinnamic acid and its derivatives. Among these, methyl cinnamate is a widely used fragrance ingredient with an annual consumption of 10–100 metric tonnes (42). Methyl *p*-chlorocinnamate is an important intermediate in the synthesis of baclofen hydrochloride, an antispastic agent (43), and the derivatives of methyl 2-naphthalate and methyl 2-quinaldic acid are also important intermediates in the synthesis of drugs. Promiscuous CbMT is rarely reported. Very recently FtpM, a fungal-derived CbMT was reported to recognize a wide range of mono and dicarboxylic acids that are distinct from its natural substrate, showing a great application potential in the production of bioplastics

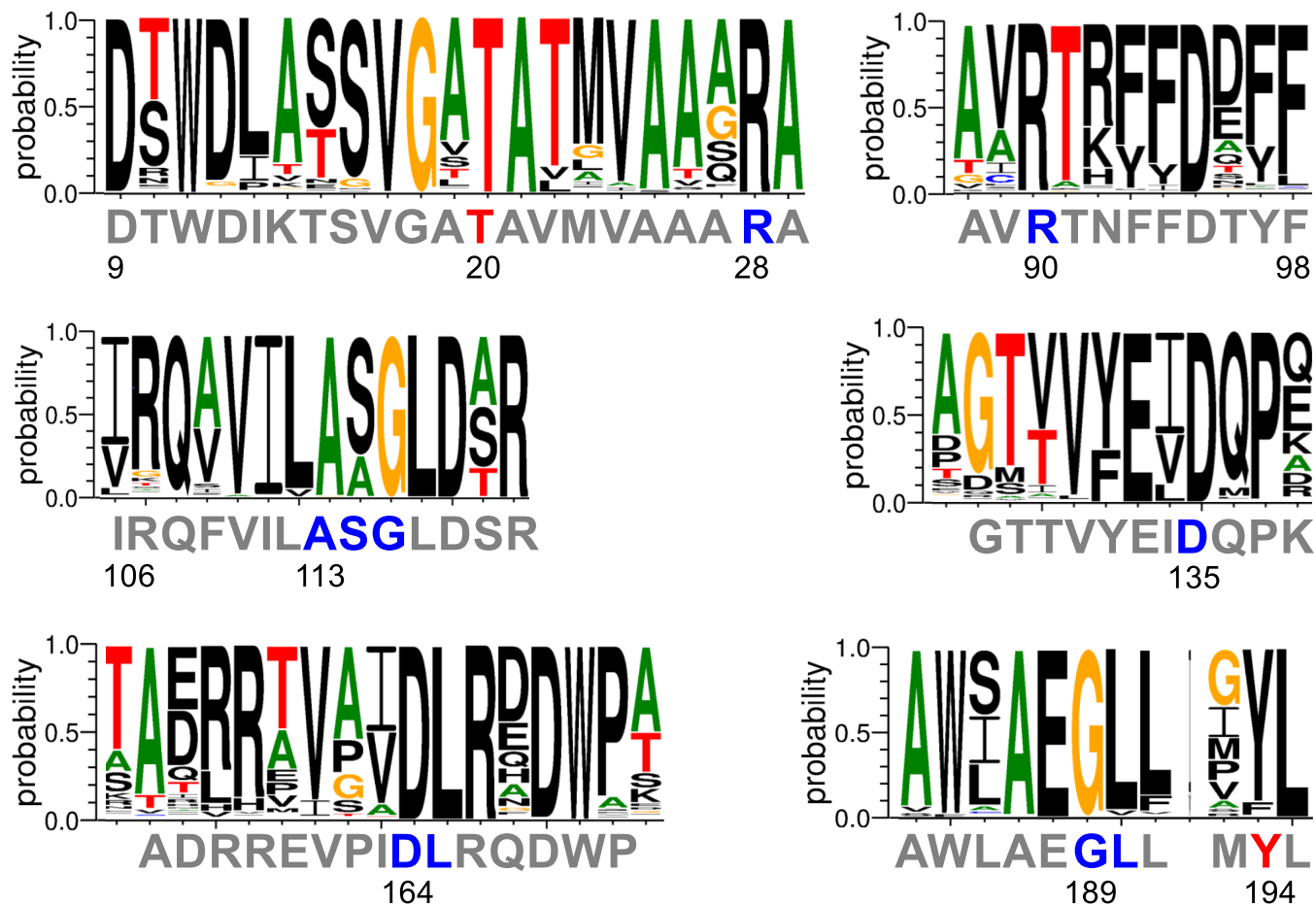


**Fig. 6.** Residue conservative analysis of more than 5,000 homologous sequences of ML2640c. The residues of ML2640c responsible for binding SAM and 3-OPC are highlighted in blue and red, respectively.

precursors (44). The catalytic efficiency of MnMT4 is at least one order of magnitude higher than that of the typical SABATH family and FtpM. In addition, efficient *in situ* regeneration of the cosubstrate SAM has been solved (45), implying that OPCMT\_like proteins can potentially be applied well in the industry as esterification tools.

Based on the homologous alignment of structure and sequence, OPCMT\_like MTs share a conserved architecture, bearing an *N*-terminal helical domain ( $\alpha_1$  to  $\alpha_4$ ) and an  $\alpha/\beta$  C-terminal domain, and the primary sequence is about 300 amino acids in length. All the structures of OPCMT\_like CbMTs reported here are monomers, different from the conventional SABATH CbMTs that exist as homodimers (17). The *N*-terminal helical domain can be recognized as an identifying feature of OPCMT\_like MTs since it has not been previously observed in other protein structures. The active residues ML2640c-T20/Y194, which are involved in the formation of critical interactions between the carboxyl-bearing substrate and SAM, are highly conserved within the OPCMT\_like MT family. The characteristics identified in this study make it easy to define more OPCMT\_like MTs. Furthermore, *in vivo* experiments showed that OPCMT\_like MTs might play an important role in maintaining homeostasis, which is indispensable to the organism, implying that the OPCMT\_like MTs could be developed as spectral antimicrobial drug targets, as they are widely and heavily present in many well-known pathogens, such as *M. tuberculosis* and *M. avium*, but are not found in the kingdom Animalia. Furthermore, according to the crystal structure of ML2640c, the substrate-binding pocket of OPCMT\_like MT is larger than that of most small-molecule

CbMTs, a feature that would facilitate the design of specific substrate inhibitors, and the atomic interactions of substrate/cofactor with ML2640c revealed here will help to improve the rationality and accuracy of the design.

## Materials and Methods

**Bacterial Strains and Plasmids.** The bacterial strains and plasmids used in this study are listed in *SI Appendix, Table S2*

**DNA Manipulation and Sequence Analysis.** DNA isolation and manipulation in *E. coli* were performed following standard methods (46). DNA polymerases (Taq and PrimeSTAR) and restriction enzymes were purchased from Takara Biotechnology (Co., Ltd. Japan) or TransGene, (Beijing, China). DNA sequencing and primer synthesis were performed by Tsingke (Shanghai, China). The primers are listed in *SI Appendix, Table S3*. Electroporation of *M. neoaurum* CCTCC AB2019054 was performed according to the procedures described previously except that the electric pulse condition was set as 2.5 kV/cm, and 25 ms (47).

**Construction and Verification of *mnmt4* Gene-Knockout Mutant of *M. neoaurum* CCTCC AB2019054.**

**Gene deletion of *mnmt4*.** The *mnmt4* gene was deleted from the chromosome of wild-type *M. neoaurum* CCTCC AB2019054 through homologous recombination. A 1.78-kb left-hand homologous fragment was amplified from the genomic DNA with two primers MnMT4-left-for/ MnMT4-left-rev. Similarly, a 1.92-kb right-hand homologous fragment was amplified with two primers MnMT4-right-for/ MnMT4-right-rev. The left fragment and the right fragment were cloned together into the *EcoRI*/ *HindIII* site of pk18mobsacB. The resulting plasmid pHZW1 was transformed into the *M. neoaurum* CCTCC AB2019054 by electroporation. Following the standard

protocol to induce the double cross-over, the *mnmt4*-deleted mutant *Mko4* was obtained. Its genotype was verified by PCR amplification using primers QC- $\Delta$ T4-for/ QC- $\Delta$ T4-rev (listed in *SI Appendix, Table S3*) and verified by DNA sequencing.

**Gene deletion of *mnmt2*.** The *mnmt2* gene was deleted from the chromosome of mutant strain *mko4* through homologous recombination. A 1.72-kb left-hand homologous fragment was amplified from the genomic DNA with two primers MnMT2-left-for/ MnMT2-left-rev. Similarly, a 1.69-kb right-hand homologous fragment was amplified with two primers MnMT2-right-for/ MnMT2-right-rev. The left fragment and the right fragment were cloned together into the *EcoRI/HindIII* site of pk18mobsacB. The resulting plasmid pHZW2 was transformed into the *mko4* by electroporation. Following the standard protocol to induce the double cross-over, the *mnmt1*-deleted mutant *mko1* was obtained. Its genotype was verified by PCR amplification using primers QC- $\Delta$ T2-for/ QC- $\Delta$ T2-rev (listed in *SI Appendix, Table S3*) and verified by DNA sequencing.

**Gene deletion of *mnmt6*.** The *mnmt6* gene was deleted from the chromosome of mutant strain *mko2* through homologous recombination. A 1.78-kb left-hand homologous fragment was amplified from the genomic DNA with two primers MnMT6-left-for/ MnMT6-left-rev. Similarly, a 1.93-kb right-hand homologous fragment was amplified with two primers MnMT6-right-for/ MnMT6-right-rev. The left fragment and the right fragment were cloned together into the *EcoRI/HindIII* site of pk18mobsacB. The resulting plasmid pHZW3 was transformed into the *mko1* by electroporation. Following the standard protocol to induce the double cross-over, the *mnmt6*-deleted mutant *mko6* ( $\Delta$ 3*mnmt*) was obtained. Its genotype was verified by PCR amplification using primers QC- $\Delta$ T6-for/ QC- $\Delta$ T6-rev (listed in *SI Appendix, Table S3*) and verified by DNA sequencing.

**Gene deletion of *mnmt3*.** The *mnmt3* gene was deleted from the chromosome of mutant strain *mko6* through homologous recombination. A 1.71-kb left-hand homologous fragment was amplified from the genomic DNA with two primers MnMT3-left-for/ MnMT3-left-rev. Similarly, a 1.78-kb right-hand homologous fragment was amplified with two primers MnMT3-right-for/ MnMT3-right-rev. The left fragment and the right fragment were cloned together into the *EcoRI/HindIII* site of pk18mobsacB. The resulting plasmid pHZW5 was transformed into the *mko6* by electroporation. Following the standard protocol to induce the double cross-over, the *mnmt3*-deleted mutant *mko9* ( $\Delta$ 4*mnmt*) was obtained. Its genotype was verified by PCR amplification using primers QC- $\Delta$ T3-for/ QC- $\Delta$ T3-rev (listed in *SI Appendix, Table S3*) and verified by DNA sequencing.

**Gene deletion of *mnmt5*.** The *mnmt5* gene was deleted from the chromosome of wild-type *M. neoaurum* CCTCC AB2019054 through homologous recombination. A 1.60-kb left-hand homologous fragment was amplified from the genomic DNA with two primers MnMT5-left-for/ MnMT5-left-rev. Similarly, a 1.65-kb right-hand homologous fragment was amplified with two primers MnMT5-right-for/ MnMT5-right-rev. The left fragment and the right fragment were cloned together into the *EcoRI/HindIII* site of pk18mobsacB. The resulting plasmid pHZW4 was transformed into *M. neoaurum* CCTCC AB2019054 by electroporation. Following the standard protocol to induce the double cross-over, the *mnmt5*-deleted mutant *mko5* was obtained. Its genotype was verified by PCR amplification using primers QC- $\Delta$ T5-for/ QC- $\Delta$ T5-rev (listed in *SI Appendix, Table S3*) and verified by DNA sequencing.

#### Site-Directed Mutagenesis of the ML2640c Protein and Enzymatic Assays

**In Vitro.** The residues tyrosine, threonine, and tryptophan of ML2640c were mutated to phenylalanine, valine, and alanine, respectively. The ML2640c-pET28a fragment was amplified by the primers (Y194F-For/ Y194F-Rev, T20V-For/ T20V-Rev, W229A-For/W229A-Rev), followed by *DpnI* digestion, resulting in the construction of recombinant plasmids (Y194F-ML260c-pET28a, T20V-ML260c-pET28a, W229A-ML260c-pET28a). Then the plasmid Y194F-ML260c-pET28a was amplified by the primer T20V-For/T20V-Rev, followed by *DpnI* digestion, resulting in the construction of the recombinant plasmid Y194F/T20V-ML260c-pET28a. The recombinant plasmid was introduced into *E. coli* BL21 (DE3) by chemical transformation. All above primers are listed in *SI Appendix, Table S3*.

The enzymatic assays of the mutant proteins were carried out at 200  $\mu$ L PBK buffer (100 mM, pH 8.0). The buffer was composed of 1 mM 3-OPC, 2 mM SAM, 10  $\mu$ M SAHE, 10  $\mu$ M LuxE, and 10  $\mu$ M mutant proteins, incubating at 37  $^{\circ}$ C for 10 min, 20 min, 0.5 h, 1 h, 4 h, 8 h and 12 h, respectively. The reaction was quenched by adding 5 times volume of methanol and then centrifuged. The supernatant was subjected to UPLC-MS analysis.

**Chemical Synthesis of 3-OPC.** The synthesis of 3-OPC was carried out according to the procedures described previously (30). A sample of 4-HBC (100 mg, 0.33 mmol) dissolved in glacial acetic acid (2.2 mL), was oxidized with  $\text{CrO}_3$  (66.6 mg, 0.66 mmol) dissolved in water (0.2 mL) and glacial acetic acid (1 mL), and the reaction mixture maintained at room temperature for 6 h. Then, 5.4 mL of ethanol was added to mixture the excess chromic acid upon cooling the solution to 5  $^{\circ}$ C. Next, 5% NaOH was added to adjust the pH to 11, and the solution was extracted with  $\text{CH}_2\text{Cl}_2$ . The organic phase was washed twice with water. The aqueous phases were combined and acidified with HCl to pH = 2 and was extracted with  $\text{CH}_2\text{Cl}_2$ . The organic phases were combined, washed with brine, and dried over anhydrous  $\text{Na}_2\text{SO}_4$ . The filtrate was concentrated under vacuum affording the product 3-OPC (80.59 mg, 71%) as a white solid.

#### The Equilibrium Dissociation Constant ( $K_D$ ) of MnMT4 with SAM and SAH.

The equilibrium dissociation constant ( $K_D$ ) of MnMT4 with SAM and SAH was performed by biolayer interferometry technology and analyzed by a ForteBio Octet RED 96 system (FortéBio, USA). All binding studies were carried out at 37  $^{\circ}$ C. Nickel affinity column (Ni-NTA) sensor was loaded with biotinylated MnMT4 (40  $\mu$ M) protein in a buffer containing 20 mM HEPES, pH 7.4, 300 mM NaCl. After reaching the baseline in the same buffer, association and dissociation were carried out with SAM and SAH, respectively. Steady-state binding responses were determined by the overall response on each sensor, and the data were analyzed using the software of Octet RED 96. In order to accurately determine the dissociation value, SAH (3, 15, 75  $\mu$ M) and SAM (1, 5, 25 nM) were used to interact with the immobilized MnMT4 protein, respectively. Steady-state binding responses were determined by the overall response on each sensor, and the data were analyzed using the software of Octet RED 96. The commercial SAM and SAH were dissolved in deionized water in these experiments.

#### Construction of Protein Expression Plasmids

The encoding genes of MnMTs were amplified by the primer pair MnMT2/3/4/5/6-For and MnMT2/3/4/5/6-Rev, using the genomic DNA of *M. neoaurum* CCTCC AB2019054 as a template. The resulting fragments were inserted into the *NdeI* and *EcoRI* sites of pET28a to afford recombinant plasmid (pET28a-MnMT2/3/4/5/6). The encoding genes of SAH nucleosidase and LuxS were amplified by the primer pair SshE-For/ SahE-Rev, LuxS-For/ LuxS-Rev, using the genomic DNA of *E. coli* BL21 (DE3) as a template. The resulting fragments were inserted into the *NcoI* and *EcoRI* sites of pET28a to afford the recombinant plasmid (pET28a-SahE and pET28a-LuxS). All primers used to construct the expression plasmids are listed in *SI Appendix, Table S3*.

**Protein Expression and Purification.** The recombinant plasmids were transferred into *E. coli* BL21 (DE3) for protein overexpression. The culture of each *E. coli* transformant was incubated in Luria-Bertani (LB) medium containing 50  $\mu$ g mL<sup>-1</sup> kanamycin at 37  $^{\circ}$ C and 220 rpm until the cell density reached 0.6 to 0.8 at OD<sub>600</sub>. Protein expression was induced by the addition of isopropyl- $\beta$ -D-thiogalactopyranoside (IPTG) to a final concentration of 0.1 mM, followed by further incubation for 20 h at 16  $^{\circ}$ C. The cells were harvested by centrifugation at 4,000 rpm for 20 min at 4  $^{\circ}$ C and were resuspended in lysis buffer (20 mM HEPES, 300 mM NaCl, 10 mM imidazole, pH 7.5). After sonication, the soluble fraction was collected and subjected to a Ni-NTA affinity column that had been equilibrated with lysis buffer, and then washed with washing buffer (20 mM HEPES, 300 mM NaCl, 50 mM imidazole, pH 7.5), followed by elution buffer (20 mM HEPES, 300 mM NaCl, 250 mM imidazole, pH 7.5). The desired protein fractions were concentrated (to 500  $\mu$ M to 1 mM) using Amicon<sup>®</sup> Ultra Centrifugal Filter Devices (Millipore, MA; molecular mass cutoff of 10 kDa for all proteins) and desalted using a PD-10 Desalting Column (GE Healthcare, USA) according to the manufacturer's protocols. The protein was stored at -80  $^{\circ}$ C in 20 mM HEPES buffer (pH 7.5) with 10% glycerol and the concentration of protein was measured by the NanoDrop3000.

**Spectroscopic Analysis.** UPLC and UPLC-MS analyses were carried out on an Apollo C18 column (1.9  $\mu\text{m}$ , 2.1 mm  $\times$  50 mm, SHIMADZU, Japan) by gradient elution of mobile phase A ( $\text{H}_2\text{O}$  supplemented with 0.1% formic acid) and mobile phase B (acetonitrile supplemented with 0.1% formic acid) using a flow rate of 0.2 mL  $\text{min}^{-1}$  over a 11 min program: 0 to 1 min, 5 to 10% phase B; 1 to 8 min, 10 to 100% phase B; 8 to 9 min, 100% phase B; 9 to 10 min, 100 to 5% phase B; 10 to 11 min, 5% phase B. The detection wavelength was 254 nm.

**In Vitro Enzymatic Assays of the OPCMT\_Like MTs.** The reaction was carried out at 200  $\mu\text{L}$  PBK buffer (100 mM, pH 8.0). The buffer is composed of 1 mM substrates, 2 mM SAM, 10  $\mu\text{M}$  SAHE, 10  $\mu\text{M}$  LuxsE, and 10  $\mu\text{M}$  OPCMTs, incubating at 37  $^\circ\text{C}$  for 0.5 h, 1 h, 4 h, 8 h, or 12 h. The 50- $\mu\text{L}$  reaction system was quenched by adding 250  $\mu\text{L}$  methanol and then centrifuged. The supernatant was subjected to UPLC-MS for analysis.

**Determination of the Enzymatic Kinetic Constants of the OPCMT\_Like MTs.** Kinetic parameters for 3-OPC were determined by monitoring the decrease of 3-OPC, using a Shimadzu UPLC system (Shimadzu, Kyoto, Japan). The area under the 3-OPC peak was converted to concentration using a 3-OPC calibration curve generated with known concentrations of standard. Based on the initial reaction rates, the apparent  $K_m$  and  $V_{\text{max}}$  values were determined using the Michaelis–Menten function of the program Graphpad Prism 5.0. Results are mean  $\pm$  SEM of triplicate experiments. (SI Appendix, Fig. S8.)

The determination of kinetic constants of MnMT4 was carried out in 200  $\mu\text{L}$  reaction volume contained PBK buffer (100 mM, pH 8.0), 0.05  $\mu\text{M}$  MnMT4, 1  $\mu\text{M}$  SAHE, 1  $\mu\text{M}$  LuxsE, 0.5 mM SAM, and different concentrations of the substrate, while the determination of kinetic constants of MnMT2/3/5/6 was carried out in 200  $\mu\text{L}$  reaction volume contained PBK buffer (100 mM, pH 8.0), 2  $\mu\text{M}$  MnMT2/3/5/6, 10  $\mu\text{M}$  SAHE, 10  $\mu\text{M}$  LuxsE, 2 mM SAM, and different concentrations. These reactions were all started by adding the enzyme to the mixture at 37  $^\circ\text{C}$  and were quenched by adding 5 times volume of methanol, and then centrifuged. The supernatants were subjected to UPLC for analysis. The detection wavelength was 254 nm.

**Molecular Dynamics (MD) Simulations of ML2640c in the Presence of the Substrate 3-OPC and SAM.** 3-OPC and SAM were parameterized, using the default setting of the ACPYPE (<https://www.bio2byte.be/acpype/>) for assigning the partial charges and atom types. MD simulations and analysis were performed using GROMACS 2018.5 (SI Appendix, Fig. S11.). The Amber14sb\_parmbsc1 force field parameters were used for protein. The system was filled with TIP3P water in a cubic box of size 80  $\text{Å} \times 80 \text{Å} \times 80 \text{Å}$ , the distance between the boundary and the protein was 10  $\text{Å}$ . The system was neutralized by addition of explicit counter ions ( $\text{Na}^+$  and  $\text{Cl}^-$ ); we

added 14  $\text{Na}^+$  counter ions. After being neutralized, the system was energy-minimized by the steepest descent method and the conjugate gradient method in which both short-range van der Waals and short-range electrostatic interactions were truncated at 14  $\text{Å}$ . The simulated annealing time was 100 ps, which was increased to 300 K in 60 ps, followed by 40-ps simulation at 300 K. After annealing simulation, the isothermal-isovolumetric ensemble (NPT) were performed under 300 K for 2 ns. The simulation was carried out for 40 ns at temperature of 300 K and pressure of 1 atm, using 1-fs time step. The velocity-rescale method was used for temperature coupling, and the Parrinello–Rahman method was employed for pressure coupling. The particle mesh Ewald (PME) method was employed for long-range electrostatic interactions. 14  $\text{Å}$  cutoff was employed for van der Waals force (VdW) and short-range coulombic interaction.

**Assays of the Crude Enzymatic Activity of  $\Delta 4mnmt$  and *M. neoaurum* CCTCC AB2019054.**  $\Delta 4mnmt$  or *M. neoaurum* CCTCC AB2019054 were inoculated into 5 mL lemco culture medium and cultured at 30  $^\circ\text{C}$ , 220 rpm. After 48 h, the cultures were transferred to 400 mL lemco culture medium according to 1% of the inoculated ratio, and cultured at 30  $^\circ\text{C}$  and 220 rpm. After 48 h, the cells were harvested by centrifugation and resuspended in 60 mL 100 mM potassium phosphate buffer (pH = 8.0). After that, the cells were broken by a high-pressure cell crusher, and 2 mL of the cell crushing solution was concentrated to 300  $\mu\text{L}$  through a ultrafiltration tube, obtaining the concentrated crude enzyme solution for activity analysis. The reaction was carried out at 200  $\mu\text{L}$  concentrated crude enzyme solution, which contained 1 mM 3-OPC, 2 mM SAM, 10  $\mu\text{M}$  LuxsE, and 10  $\mu\text{M}$  SAHE, incubating at 37  $^\circ\text{C}$  for 0.5 h, 1 h, or 4 h. 50  $\mu\text{L}$  reaction system was quenched by adding 250  $\mu\text{L}$  methanol, and then centrifuged. The supernatant was subjected to UPLC-MS for analysis (SI Appendix, Fig. S15).

**Data, Materials, and Software Availability.** All study data are included in the article and/or SI Appendix.

**ACKNOWLEDGMENTS.** We thank Mr. Guangjun Li for the help of molecular dynamics simulations; Dr. Libing Shen for the help of the alignment of 5000 OPCMT\_like proteins' sequences. This work was supported in part by the National Key R&D Program of China (2021YFC2100600 to Z.L., 2018YFA0900400 to X.Q.), the NSFC (31770063 to X.Q. and 22107069 to Z.L.).

Author affiliations: <sup>a</sup>State Key Laboratory of Microbial Metabolism, School of Life Science & Biotechnology, Shanghai Jiao Tong University, Shanghai 200240, China; <sup>b</sup>Zhangjiang Institute for Advanced Study, Shanghai Jiao Tong University, Shanghai 200240, China; <sup>c</sup>Key Laboratory of Combinatorial Biosynthesis and Drug Discovery Ministry of Education & Abiochem Biotech Joint Center for Pharmaceutical Innovation, School of Pharmaceutical Sciences, Wuhan University, Wuhan 430071, China; and <sup>d</sup>Department of Gastroenterology and Hepatology, Tongji Hospital affiliated to Huazhong University of Science and Technology, Wuhan 430071, China

1. D. K. Liscombe, G. V. Louie, J. P. Noel, Architectures, mechanisms and molecular evolution of natural product methyltransferases. *Nat. Prod. Rep.* **29**, 1238–1250 (2012).
2. D. Dominissini *et al.*, The dynamic N(1)-methyladenosine methylome in eukaryotic messenger RNA. *Nature*. **530**, 441–446 (2016).
3. E. Abdelraheem *et al.*, Methyltransferases: Functions and applications. *ChemBioChem* **23**, e202200212 (2022).
4. D. K. Liscombe, P. J. Facchini, Molecular cloning and characterization of tetrahydroprotoberberine *cis-N*-methyltransferase, an enzyme involved in alkaloid biosynthesis in *opium poppy*. *J. Biol. Chem.* **282**, 14741–14751 (2007).
5. C. C. Huang *et al.*, Crystal structures of mycolic acid cyclopropane synthases from *Mycobacterium tuberculosis*. *J. Biol. Chem.* **277**, 11559–11569 (2002).
6. H. Coirer *et al.*, Methylation of sulfhydryl groups: A new function for a family of small molecule plant O-methyltransferases. *Plant J.* **46**, 193–205 (2006).
7. J. W. Schmidberger, A. B. James, R. Edwards, J. H. Naismith, D. O'Hagan, Halomethane biosynthesis: Structure of a SAM-dependent halide methyltransferase from *Arabidopsis thaliana*. *Angew. Chem. Int. Ed.* **49**, 3646–3648 (2010).
8. C. Lomax *et al.*, Methylated arsenic species in plants originate from soil microorganisms. *New Phytol.* **193**, 665–672 (2012).
9. J. Qin *et al.*, Arsenic detoxification and evolution of trimethylarsine gas by a microbial arsenite S-adenosylmethionine methyltransferase. *Proc. Natl. Acad. Sci. U.S.A.* **103**, 2075–2080 (2006).
10. J. Zhang, Y. G. Zheng, SAM/SAH analogs as versatile tools for SAM-dependent methyltransferases. *ACS Chem. Biol.* **11**, 583–597 (2016).
11. J. Lee, J. Stock, Protein phosphatase 2A catalytic subunit is methyl-esterified at its carboxyl terminus by a novel methyltransferase. *J. Biol. Chem.* **268**, 19192–19195 (1993).
12. V. Stanevich *et al.*, The structural basis for tight control of PP2A methylation and function by LCMT-1. *Mol. Cell.* **41**, 331–342 (2011).
13. P. T. Männistö, S. Kaakkola, Catechol-O-methyltransferase (COMT): Biochemistry, molecular biology, pharmacology, and clinical efficacy of the new selective COMT inhibitors. *Pharmacol. Rev.* **51**, 593–628 (1999).
14. Z. Ma, H. Liu, B. Wu, Structure-based drug design of catechol-O-methyltransferase inhibitors for CNS disorders. *Br. J. Clin. Pharmacol.* **77**, 410–420 (2014).

15. L. C. Ward, H. V. McCue, A. J. Carnell, Carboxyl methyltransferases: Natural functions and potential applications in industrial biotechnology. *ChemCatChem*. **13**, 121–128 (2020).
16. J. C. D'Auria, F. Chen, E. Pichersky, Chapter eleven the SABATH family of MTS in *Arabidopsis thaliana* and other plant species. *Recent Adv. Phytochem.* **37**, 253–283 (2003).
17. C. Zubieta *et al.*, Structural basis for substrate recognition in the salicylic acid carboxyl methyltransferase family. *Plant Cell*. **15**, 1704–1716 (2003).
18. L. M. Murfitt, N. Kolosova, C. J. Mann, N. Dudareva, Purification and characterization of *S*-adenosyl-L-methionine:benzoic acid carboxyl methyltransferase, the enzyme responsible for biosynthesis of the volatile ester methyl benzoate in flowers of *Antirrhinum majus*. *Arch. Biochem. Biophys.* **382**, 145–151 (2000).
19. J. Kapteyn *et al.*, Evolution of cinnamate/*p*-coumarate carboxyl methyltransferases and their role in the biosynthesis of methylcinnamate. *Plant Cell*. **19**, 3212–3229 (2007).
20. N. Zhao *et al.*, Structural, biochemical, and phylogenetic analyses suggest that indole-3-acetic acid methyltransferase is an evolutionarily ancient member of the SABATH family. *Plant Physiol.* **146**, 455–467 (2008).
21. M. Varbanova *et al.*, Methylation of gibberellins by *Arabidopsis* GAMT1 and GAMT2. *Plant Cell*. **19**, 32–45 (2007).
22. H. S. Seo *et al.*, Jasmonic acid carboxyl methyltransferase: A key enzyme for jasmonate-regulated plant responses. *Proc. Natl. Acad. Sci. U.S.A.* **98**, 4788–4793 (2001).
23. J. Murata, J. Roepke, H. Gordon, V. De Luca, The leaf epidermome of *Catharanthus roseus* reveals its biochemical specialization. *Plant Cell*. **20**, 524–542 (2008).
24. Y. Yang *et al.*, An *Arabidopsis thaliana* methyltransferase capable of methylating farnesoic acid. *Arch. Biochem. Biophys.* **448**, 123–132 (2006).
25. Y. Akamatsu, J. H. Law, The enzymatic synthesis of fatty acid methyl esters by carboxyl group alkylation. *J. Biol. Chem.* **245**, 709–713 (1970).
26. P. Nawabi, S. Bauer, N. Kyrpidis, A. Lykidis, Engineering *Escherichia coli* for biodiesel production utilizing a bacterial fatty acid methyltransferase. *Appl. Environ. Microbiol.* **77**, 8052–8061 (2011).
27. N. Petronikolou, S. K. Nair, Biochemical studies of mycobacterial fatty acid methyltransferase: A catalyst for the enzymatic production of biodiesel. *Chem. Biol.* **22**, 1480–1490 (2015).
28. N. Petronikolou, A. J. Hollatz, M. A. Schuler, S. K. Nair, Loganic acid methyltransferase: Insights into the specificity of methylation on an iridoid glycoside. *ChemBioChem* **19**, 784–788 (2018).
29. E. Jongedijk *et al.*, Novel routes towards bioplastics from plants: elucidation of the methylperillate biosynthesis pathway from *Salvia dorisiana* trichomes. *J. Exp. Bot.* **71**, 3052–3065 (2020).
30. H. Peng *et al.*, A dual role reductase from phytosterols catabolism enables the efficient production of valuable steroid precursors. *Angew. Chem. Int. Ed.* **60**, 5414–5420 (2021).
31. T. Paysan-Lafosse *et al.*, InterPro in 2022. *Nucleic Acids Res.* **51**, D418–D427 (2022), 10.1093/nar/gkac993.
32. N. Leulliot *et al.*, Structure of protein phosphatase methyltransferase 1 (PPM1), a leucine carboxyl methyltransferase involved in the regulation of protein phosphatase 2A activity. *J. Biol. Chem.* **279**, 8351–8358 (2004).
33. E. R. Jr Rafanan, C. R. Hutchinson, B. Shen, Triple hydroxylation of tetracenomycin A2 to tetracenomycin C involving two molecules of O(2) and one molecule of H(2)O. *Org. Lett.* **2**, 3225–3227 (2000).
34. C. L. Hendricks, J. R. Ross, E. Pichersky, J. P. Noel, Z. S. Zhou, An enzyme-coupled colorimetric assay for *S*-adenosylmethionine-dependent methyltransferases. *Anal. Biochem.* **326**, 100–105 (2004).
35. K. A. Cornell, W. E. Swarts, R. D. Barry, M. K. Riscoe, Characterization of recombinant *Escherichia coli* 5'-methylthioadenosine/*S*-adenosylhomocysteine nucleosidase: Analysis of enzymatic activity and substrate specificity. *Biochem. Biophys. Res. Commun.* **228**, 724–732 (1996).
36. M. Graña *et al.*, The crystal structure of *M. leprae* ML2640c defines a large family of putative *S*-adenosylmethionine-dependent methyltransferases in mycobacteria. *Protein Sci.* **16**, 1896–1904 (2007).
37. J. L. Martin, F. M. McMillan, SAM (dependent) I AM: The *S*-adenosylmethionine-dependent methyltransferase fold. *Curr. Opin. Struct. Biol.* **12**, 783–793 (2002).
38. L. R. Jarboe, L. A. Royce, P. Liu, Understanding biocatalyst inhibition by carboxylic acids. *Front. Microbiol.* **4**, 272 (2013).
39. J. C. Chang *et al.*, Igr genes and *Mycobacterium tuberculosis* cholesterol metabolism. *J. Bacteriol.* **191**, 5232–5239 (2009).
40. E. Y. Bragin *et al.*, Comparative analysis of genes encoding key steroid core oxidation enzymes in fast-growing *Mycobacterium* spp. strains. *J. Steroid Biochem. Mol. Biol.* **138**, 41–53 (2013).
41. Y. Tong *et al.*, CRISPR-Cas9, CRISPRi and CRISPR-BEST-mediated genetic manipulation in streptomycetes. *Nat. Protoc.* **15**, 2470–2502 (2020).
42. S. P. Bhatia *et al.*, Fragrance material review on methyl cinnamate. *Food Chem. Toxicol.* **45**, S113–S119 (2007).
43. P. J. Kitson *et al.*, Digitization of multistep organic synthesis in reactionware for on-demand pharmaceuticals. *Science* **359**, 314–319 (2018).
44. L. C. Ward *et al.*, Carboxyl methyltransferase catalyzed formation of mono- and dimethyl esters under aqueous conditions: Application in cascade biocatalysis. *Angew. Chem. Int. Ed.* **61**, e202117324 (2022).
45. X. Wen, F. Leisinger, V. Leopold, F. P. Seebeck, Synthetic reagents for enzyme-catalyzed methylation. *Angew. Chem. Int. Ed.* **61**, e202208746 (2022).
46. J. Sambrook, D. W. Russell, *Molecular Cloning: A Laboratory Manual* (Cold Spring Harbor Laboratory Press, New York, ed. 3, 2001).
47. B. H. Kvitko, A. Collmer, Construction of *Pseudomonas syringae* pv. tomato DC3000 mutant and polymutant strains. *Methods Mol. Biol.* **712**, 109–128 (2011).